

# A COMPUTATIONAL STUDY OF SCRAMJET COMBUSTION

C. Fureby, M. Chapuis, E. Fedina & J. Tegnér

Defense Security Systems Technology, The Swedish Defense Research Agency – FOI, Stockholm, Sweden

**Keywords:** *scramjet combustion, large eddy simulation, self-ignition, flame stabilization*

## Abstract

*The development of scramjet propulsion systems requires experimental and numerical studies to interlace and help understand the complex flow physics and its interactions with the thermomechanics of the engine, and ultimately to help guide the design. Here, Large Eddy Simulation (LES) is used to analyze supersonic flow, mixing, self-ignition and combustion in a laboratory supersonic combustor and in the HyShot II scramjet combustor. The focus of this study is to further validate the LES combustion model and to study two different flame stabilization mechanisms. The laboratory scramjet combustor uses a strut injector whereas the HyShot scramjet engine makes use of a jet-in-cross flow injector. Comparison with experimental data shows that the LES model, together with an eight step reduced H<sub>2</sub>-air mechanism, is able to capture different types of self-ignition and supersonic combustion, and the predictions are used together with the experimental data to further elucidate the complex reacting flow in these two scramjet combustors. New knowledge about self-ignition and flame stabilization mechanisms is obtained that qualitatively agrees well with existing experimental data.*

## 1. Introduction and Background

The development of reliable hypersonic flight vehicles requires the solution of many challenging technical problems associated with the comparatively small net thrust at supersonic flight velocities. A key air-breathing propulsion challenge is the design of a robust engine capable of operating over the large flight Mach number range of high-speed flight and space access vehicles. The development of such propulsion systems

requires both experimental and numerical studies to interlace in order to help understand the complex flow physics and its interactions with the thermo-mechanics of the engine, and ultimately to help guide the design. Conventional Reynolds Averaged Navier Stokes (RANS) models, with simplified combustion models, [1], usually provide no more than guidelines to the design of experimental rigs and the overall goal of using a numerical predictive capability to simulate actual flight conditions still remains unreached. More recently, Large Eddy Simulation (LES) models, [2-3], have been proposed as a promising alternative, having potential to provide both qualitative and quantitative data that can help understand the flow physics and provide reliable predictions as required in the detailed design process. However, for LES to be useful for the study of such flows, further advancement in subgrid flow, combustion closures and numerical methods as well as parallel simulation strategy are needed.

In this investigation we use a combustion LES model together with a reduced hydrogen air reaction mechanism to investigate supersonic combustion in a laboratory supersonic combustor, [4], and in the HyShot II scramjet engine, [5]. The simulation of the laboratory supersonic combustor aims at characterizing fuel-injection, mixing, self-ignition, flame stabilization and turbulent combustion in supersonic flows – usually of a different nature than in subsonic combustion as the air speed is significantly higher than the turbulent flame speed. The understanding of these phenomena is very important for understanding supersonic combustion and thus of developing future scramjet engines. An additional objective is to provide additional validation of the combustion LES model. The simula-

tion of the HyShot II scramjet engine is intended to facilitate a detailed description of the fuel-injection, mixing, self-ignition, flame stabilization and turbulent combustion under flight-like conditions. Flight test data, [6], and experimental data from the High Enthalpy Shock Tunnel Göttingen (HEG) of the German Aerospace Centre (DLR), [7], in particular, will aid in validating the computational model and guide the analysis.

## 2. Mathematical and Numerical Modeling

The mathematical model used consists of the balance equations of mass, species mass fractions, momentum and energy, describing convection, diffusion and reactions, [8]. The reactive gaseous mixture is assumed to be a linear viscous fluid with Fourier heat conduction and Fickian diffusion, [9]. The viscosity is computed from Sutherland's law and the thermal conductivity and species diffusivities are computed using the viscosity and constant Prandtl and species Schmidt numbers, respectively. The mixture thermal and caloric equations of state are obtained under the assumption that each specie is a thermally perfect gas, with tabulated formation enthalpies and specific heats, respectively, [9]. The reaction rates are computed from Guldberg-Waage's law of mass action by summation over all participating reactions, with rate constants obtained from a modified Arrhenius law, [10]. The ranges of scales present in turbulent reacting flows typically covers eight orders of magnitude, [11], with the smaller scales being less energetic but important for the chemical kinetics. In this study, the Large Eddy Simulation (LES) model, [3], is used to simulate both combustors, [4] and [5-7], using the mixed sub-grid scale flow model, [12], and the Partially Stirred Reaction (PaSR) turbulence chemistry interaction model, [13]. The LES equations are solved using a fully explicit finite volume discretization, using the C++ library OpenFOAM, [14], together with a two-stage Runge-Kutta time-integration scheme. Hydrogen ( $H_2$ ) is used as fuel in both supersonic combustors studied, and the combustion chemistry used is the 7-species and 8-step reduced reaction mechanism of Davidenko *et al*, [15].

## 3. Validation and Supersonic Combustion Characteristics

Prior to performing an analysis of the flow, fuel injection, mixing, self-ignition and combustion of  $H_2$  in the HyShot II scramjet engine, self-ignition of  $H_2$  in vitiated hot confined supersonic air flow, corresponding to the experiments of Sunami *et al*, [4], has been investigated. The motivation for this work has been to further validate the finite rate chemistry LES model and to enhance our understanding of the key physical processes, [3]. Figure 1a shows a photograph of the laboratory combustion facility, consisting of the NAL supersonic combustor, [16], connected to the LAERTE vitiation air heater, [17]. The combustor is composed of a 0.36 m long constant area duct with a cross section of  $0.05 \times 0.10 \text{ m}^2$  followed by a 0.60 m long diverging area duct, having upper and lower expansion angles of  $1.72^\circ$ , respectively. To have optical access, quartz windows cover the sides of the combustor, whereas pressure transducers are arranged along the centerline of the upper combustor wall. The ONH10 two-stage injection strut used here includes a first row of  $4 \times \phi 2.0 \text{ mm}$   $45^\circ$  slanted Ma 2.5 injectors on the top and bottom walls of the strut, 27 mm from its base and a second row of  $3 \times \phi 4.3 \text{ mm}$  horizontal Ma 2.5 injectors on the strut base, 0.433 m downstream of the combustor entrance. The injectors have a spacing of 25 mm, with the second row of injectors located between the rows of the first stage injectors. Gaseous  $H_2$  at 124 K is feed into the  $O_2/N_2/H_2O$  mixture at 2149 m/s with a mass fraction distribution of 0.23:0.70:0.07, at a density of  $0.1335 \text{ kg/m}^3$ , a temperature of 830 K, a velocity of 1449 m/s, and a pressure of 34.2 kPa. The  $H_2$  mass flow distribution between the first and the second stage injectors is 40% and 60%, respectively. The computational model spans the entire combustor using a coarse grid of 9 Mcells and a fine grid of 72 Mcells. Dirichlet boundary conditions are used for all variables at the inlets, whereas at the outlet, all variables are extrapolated. At the walls, a no-slip wall model, [18], is applied together with zero Neumann conditions for all other variables.

From the experimental study, [4], it is clear that close to the injection strut (40 mm down-

stream of the strut trailing edge) OH emission due to combustion is clearly seen at four span-wise locations corresponding to the first stage  $H_2$  injectors between the parallel  $H_2$  jets of the second stage injection from the strut base. This demonstrates successful ignition by the first stage injection. Ignition of the second stage  $H$  jets can also be observed in a spotty pattern around the second stage  $H_2$  jets. Further downstream (at 100 mm downstream of the strut trailing edge) the OH emission due to combustion is found to have a spotty character and now appears in the form of random pockets connected by weaker values of OH. The intensity appears highly unsteady and it is clear that turbulence of a wide range of scales strongly influences the combustion process. By comparing with the measured wall pressure distribution it is evident that the pressure peaks at about 80 mm downstream of the strut trailing edge due to extensive volumet-

ric expansion. Spontaneous flame images, figure 1b, shows a flame gradually growing in thickness in the strut wake until it widens about 90 mm downstream of the strut trailing edge. This blunt flame front oscillates back and forth, having an amplitude of 40 mm, and hence separate into an upper and lower branch about 140 mm downstream of the strut trailing edge.

Figure 1c shows a perspective view of the predicted flow in the combustor. The numerical schlieren show oblique shocks at the leading edge of the strut, reflecting first in the combustor wall, then in the strut, and again in the combustor wall before impinging on the flame. Together with the weakly bend expansion fans originating at the trailing edges of the injection strut, this causes a distinctive shock-wave pattern to develop further downstream in the diverging area combustor.

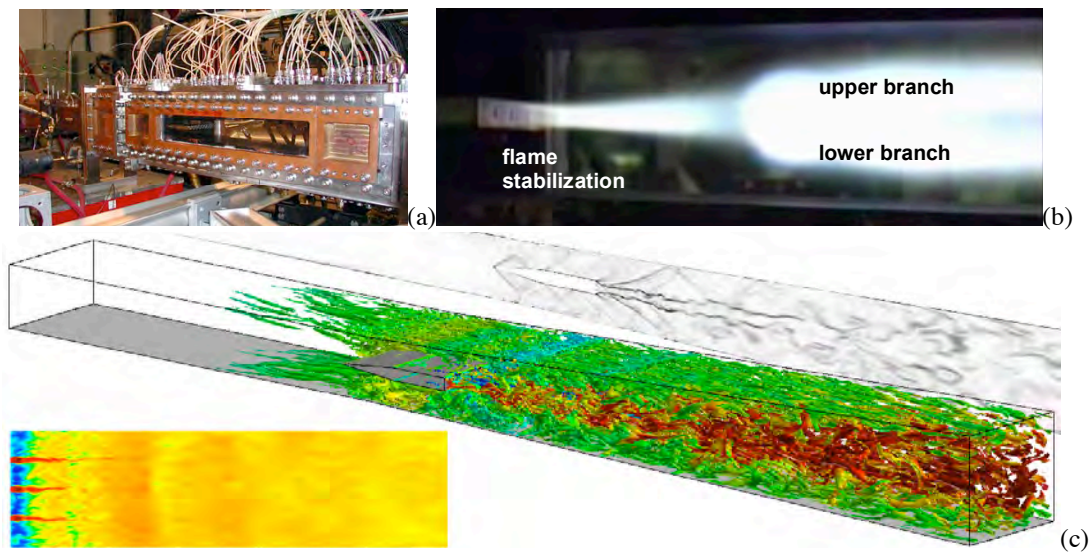


**Figure 1.** Photograph (a) of the NAL supersonic combustor, (b) experimental spontaneous flame images and (c) a perspective view of the flow in terms of iso-surfaces of the second invariant of the velocity gradient tensor colored by the temperature together with a numerical schlieren image (top) and centerplane contours of the axial velocity (bottom).

At the walls, the boundary layer thickens and the fluctuations increase as a consequence of the shock-boundary layer interactions. The boundary layers of the strut separate at the strut base to develop unstable shear-layers that break-up and develop Kelvin Helmholtz (KH) vortices that are advected further downstream whilst interacting with the high-speed flow, the shock-wave pattern and the high temperature (or

flame) region. From figure 1c it is evident that the high temperature region downstream of the injection strut is topologically complex due to the large amount of in-tense coherent vortex structures, responsible for species and thermal mixing as well as energy re-distribution, forming the flow downstream of the injection strut. This vortical high-temperature region is further modified by the impinging shock and rarefac-

tion waves, resulting in agglomeration of vortex structures in outer high temperature region due to shock-vortex interactions. This agglomeration of vortex structures further enhances species and thermal mixing which in turn is believed to facilitate additional chemical reactions. The centerplane velocity distribution in figure 1c reveals a short recirculation region just downstream of the injection strut, interrupted only by the Ma 2.5 H<sub>2</sub> jets. The fact that the flame is stabilized in this very high-speed flow indicates that it is not an ordinary flame but rather a sequence of self-ignition events.

Comparisons of predicted and measured centerline wall pressure and OH emissions from combustion 40 and 100 mm downstream of the strut trailing edge are shown in figure 2. The first wall pressure rise (at  $x \approx 0.30$  m) is due to the incident shock wave originating from the strut leading edge into the combustor wall bound-

dary layer, whereas the second peak is due to the fuel injection. Just downstream of the strut trailing edge (at  $x \approx 0.43$  m) we find a dramatic increase in pressure for the reacting case compared to the case without H<sub>2</sub> injection. This pressure increase is characteristic of successful combustion and is due to the volumetric expansion caused by heat release from the chemical reactions. Good agreement between predictions and experimental data is observed for both the non-reacting and reacting case. The comparison of predicted instantaneous and time averaged OH emissions at  $x=0.473$  m and  $x=0.543$  m, shown in figures 2b to 2e also show good agreement between predictions and experimental data, indicating that the PaSR-LES model is capable of predicting the experimentally observed highly fragmented OH distribution that is typical of self-ignition as observed experimentally by George *et al*, [19].

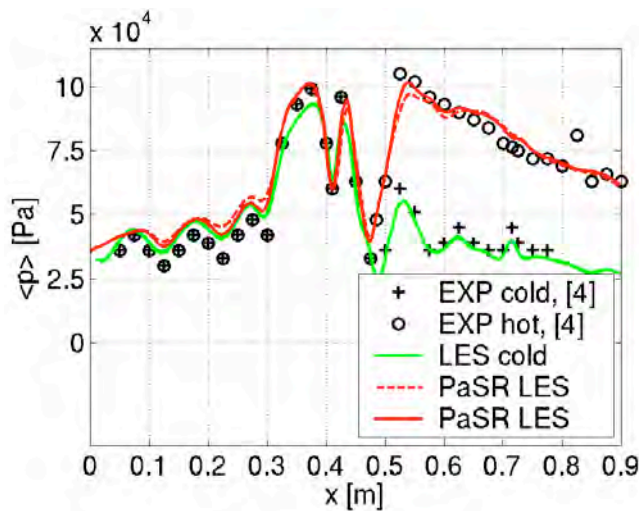


**Figure 2.** Comparison of predicted and measured wall pressure (a) and comparison of instantaneous (left) and time averaged (right) OH emissions at 40 mm downstream of the strut trailing edge from (b) experiments and (c) PaSR-LES and 100 mm downstream of the strut trailing edge from (d) experiments and (e) PaSR-LES.

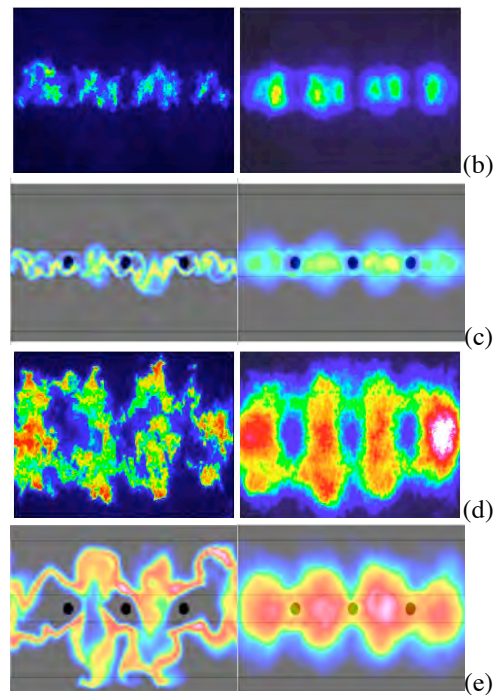
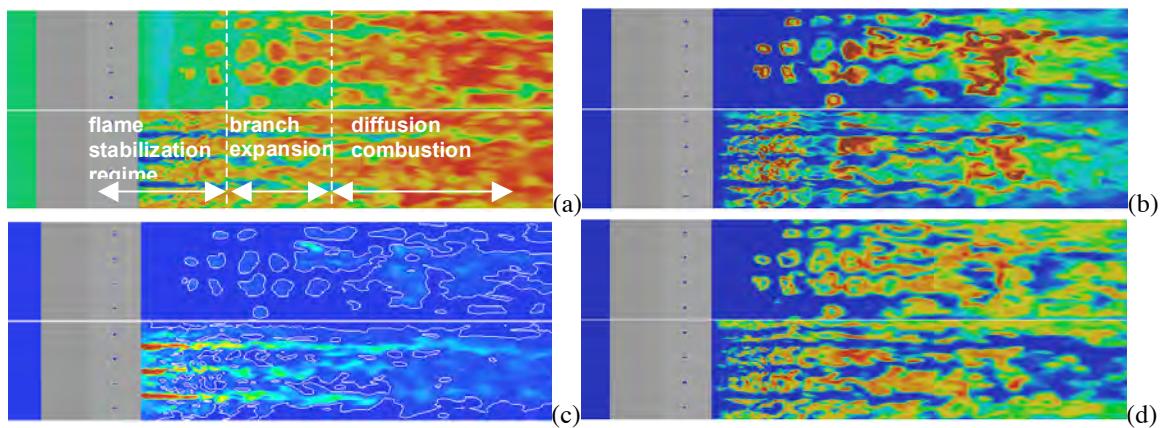


Figure 3 presents instantaneous (a) temperature, (b) heat-release, (c) mixture fraction and (d) OH distributions at the combustor centerplane (through the H<sub>2</sub> jets) and 5.0 mm below the injection strut, respectively. These distributions, together with the instantaneous velocity distribution in figure 1c, are consistent with the experimentally observed flame behavior in figure 1b, in which the initially narrow flame rap-

idly widen at about 0.09 m downstream of the strut trailing edge to subsequently separate into an upper and lower branch at about 0.14 m downstream of the strut trailing edge. The flame anchors in the narrow high-speed flow region just downstream of the injection strut, with chemical reactions taking place in fragmented pockets between the primary H<sub>2</sub> jets. These pockets contain H<sub>2</sub> from the first row of injectors, and

self-ignite as a consequence of the high temperature in combination with high levels of H that stimulate self-ignition through the chain-branching step  $\text{H} + \text{O}_2 \rightleftharpoons \text{OH} + \text{O}$ , the products of which react with  $\text{H}_2$  to produce H, which continues to react, producing even more radicals, until the resulting pool of radicals reaches a critical level, whereby a very rapid exothermic reaction occurs. In this flame stabilization region heat-release occurs in fragmented pockets, uncorrelated with the stoichiometric mixture fraction, where the temperature is high enough, and the

species are sufficiently well mixed to facilitate self-ignition and very rapid burning. Downstream of the combined self-ignition and flame stabilization region the flame change character and heat is instead primarily released in an upper and lower branch (cf figure 3b). In this turbulent combustion region, the heat release correlates reasonably well with the stoichiometric mixture fraction in the upper and lower branches, suggesting that combustion in this regime is similar to a turbulent diffusion flame.



**Figure 3.** Instantaneous distributions of (a) temperature, (b) heat release, (c) mixture fraction and (d) OH at the centerplane (bottom) and 5 mm below the lower side of the injection strut (top).

#### 4. The HyShot II Combustor

A more realistic model of a working scramjet engine is the well-known HyShot II combustor, [5], for which laboratory data, [7], and flight test data exists, [6], for similar conditions. Here we focus on investigating the 1:1 scale model of the HyShot II vehicle, [7], numerically studied by Karl *et al*, [20], using RANS. The main reason for this choice is that this ground-based experiment provides a more exhaustive data set than the HyShot II scramjet flight test, devised to achieve supersonic combustion in flight above Mach 7.5 using a ballistic reentry vehicle.

The computational model of the HyShot II scramjet combustor is shown in figure 4. At the inflow ( $x=0.360$  m) Dirichlet conditions are used for all variables with profiles resulting from the test-section simulation. Isothermal no-slip wall boundary conditions are used to represent the top and bottom walls of the combustor

whereas symmetry conditions are used in the spanwise direction, thus neglecting the influence of the side-walls. The wall temperature is fixed to 300 K to account for the short test time in the HEG facility. The exhaust nozzle was only partially included up to a plane 0.110 m downstream of the end of the combustion chamber (at  $x=0.760$  m) at which all variables are extrapolated. Fuel injection was modeled by partially including the injectors using a total hydrogen pressure of 297 kPa and a total temperature of 300 K at the injector inflow. For the HEG experiment simulations the global equivalence ratio was  $\phi=0.43$  but for the flight-tests it was slightly lower. The RANS computations, [20], take advantage of all symmetries of the combustor and hence only one quarter of the computational domain shown in figure 4 was modeled, whereas in the present LES the full domain in figure 4 is modeled. For LES structured grids with 12 and 25 Mcells are used. Grid refinement studies have been performed, indicating that the

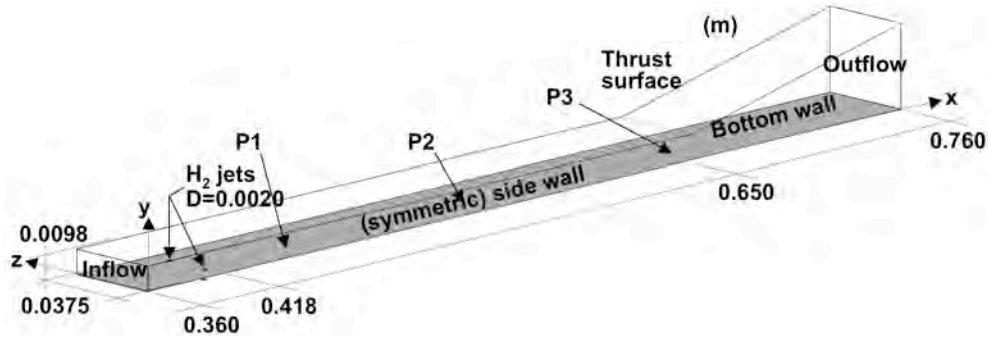


**Figure 4.** Computational model of the HyShot II combustor used in the LES analysis.

grids used are sufficiently fine to capture the most important flow features.

The composite figure 5 presents selected aspects of the reacting flow in the HyShot II combustor from the LES. This figure shows (a) the wall pressure together with an iso-surface of the  $H_2$  mass fraction, (b) an axial velocity cut through one of the fuel injectors, (c) an iso-surface of the second invariant of the velocity gradient,  $\lambda_2$ , colored by the temperature, and (d) iso-surfaces of the  $H_2$  mass fraction (gray) and the heat release conditioned on  $\lambda_2$ . The wall pressure in figure 5a reveals that initially the pressure increases slowly with increasing distance from the transverse  $H_2$  jets to rapidly increase between 30 and 60D downstream of the transverse  $H_2$  jets to peak at about 100D. Higher wall pressures are also observed beneath the bow shock, forming a hood over the transverse fuel jet and beneath the fuel jets. The more rapid

pressure increase further downstream is caused by volumetric expansion due to exothermicity and chemical reactions. The large diffusivity of  $H_2$  allows it to rapidly mix with the freestream air, forming a reactive mixture around the high momentum  $H_2$  filled jet core seen in figure 5c.

The velocity in figure 5b shows the high speed ( $Ma \approx 7.2$ ) flow entering the combustor, the transverse  $H_2$  jet, the bow shock and the complex flow structures developing downstream of the injection points. The jet-to-freestream momentum flux ratio is  $J \approx 1.1$  and the mean  $H_2$  jet penetration profile is close to that proposed by Gruber *et al*, [21], and the  $H_2$  jets are observed to penetrate to  $\sim 30\%$  of the combustor height before self-ignition. The axial velocity in the combustor is slightly reduced compared with that at the inflow due to the combined blocking and redirection effects caused by the transverse jets. The flame is anchored by the

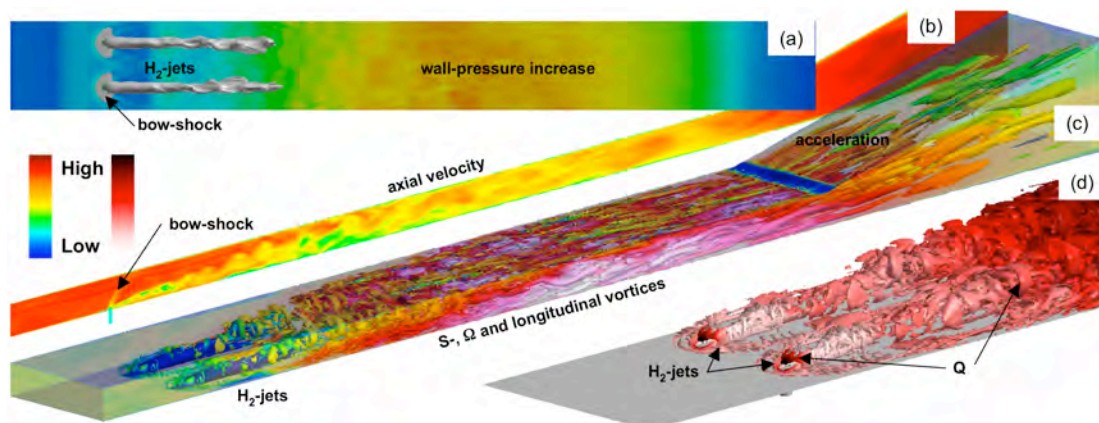


**Figure 5.** Composite figure of the reacting flow in the HyShot II combustor: (a) wall pressure and an iso-surface of the  $H_2$  mass fraction, (b) axial velocity cut through a fuel injector, (c) iso-surface of the second invariant of the velocity gradient,  $\lambda_2$ , colored by the temperature and (d) iso-surfaces of the  $H_2$  mass fraction (gray) and the heat release conditioned on  $\lambda_2$ .

intermittent wakes, formed behind the jets, and the recirculation of hot combustion products. In the second half of the combustor the flow accelerates due to the volumetric expansion. The time-averaged transverse  $H_2$  jets typically consist of a counter-rotating vortex pair and a horseshoe-vortex, whereas instantaneously they consist of smaller and topologically more complex vortex structures, cf. figure 5c. These typically consist of small bent S-shaped vortices (or side arms) with their lower parts aligned with the flow and their upper parts curling over the jet forming the neck (circumferential rollers) of the counter-rotating vortex pair. This feature is observed experimentally by Ben-Yakar *et al*, [22], and they propose that the side arms are stretched by increased shear stresses in the regions of steep velocity gradient. These vortical structures seem to arise from Kelvin-Helmholtz (KH) instabilities in the jet shear layers just beneath the bow-shock. Since the transverse jets contain all the  $H_2$ , mixing dominates during the first 20 to 40D, whereby air is entrained into the vortex structures and  $H_2$  diffuses into the air, resulting in a combustible mixture around the jets. Further downstream, between 30 and 60D the  $H_2$  and air are sufficiently mixed to burn if the temperature is sufficiently high. In this region, self-ignition occurs intermittently with the assistance of hot recirculated products and appears to be triggered by hot-spots in regions of colliding shocks which hence explains the unsteady nature of the self-ignition region. The volumetric expansion causes the S-shaped side arms and spanwise rollers to combine into  $\Omega$ -shaped vortices, dominating the self-ignition region. Due to volumetric expansion, vortex stretching, baroclinic torque and self-diffusion, the vortex structures eventually develop into longitudinal vortices, dominating the downstream part of the combustor. These vortices grow in size with increasing distance from the injection point due to the volumetric expansion, and when they reach the end of the combustor, the gradual expansion increases the velocity, presented in figure 5b, causing a forward directed thrust on the thrust surface.

In figure 5d the iso-surfaces of the  $H_2$  mass fraction (gray) and the heat release, defined as

the source term in the transport equation for the sensible enthalpy, [9], conditioned on  $\lambda_2$  support the previous description of the self-ignition process. Heat release occurs locally beneath the bow-shock as  $H_2$  and air are mixed when the transverse  $H_2$  jets impinge on the airflow through the combustor however the heat release ceases further downstream, between 10 and 25 D, due to insufficient mixing. Further downstream, where  $H_2$  and air are well mixed, self-ignition, aided by recirculated combustion products, due mainly to interacting shocks, occurs, causing the S-shaped vortices and the spanwise rollers to rapidly develop  $\Omega$ -shaped vortices. The chain-branching step  $H+O_2 \rightleftharpoons OH+O$  is very important for self-ignition as its products react with  $H_2$  to produce H, that continues to react, producing more radicals, until the resulting pool of radicals reaches a critical level, whereby a rapid exothermic reaction occurs.

In figure 6 predicted and measured axial profiles of (a) the time-averaged wall pressure,  $\langle \bar{p} \rangle$ , and (b) wall heat flux,  $\langle \bar{h} \rangle$ , are compared. The wall pressure and heat flux are compared at lines on the bottom wall of the combustor between injectors and 6.0 mm off centerline between injectors, respectively. For the time-averaged wall pressure the experimental data show a sudden increase between  $x=0.50$  and  $0.53$  followed by a slower increase up to the end of the combustor, at  $x=0.65$ , after which the pressure drops rapidly to the exit pressure. The RANS predictions show an almost linear increase from the combustor inlet to the combustor exit, missing the sharp pressure increase indicating combustion, and under- or overpredicting the wall pressure by up to 25%. The LES predictions are in better qualitative agreement with the experimental data, in particular showing a pressure rise although in two phases and starting somewhat too early. This indicates that LES is able of capturing mixing, self-ignition and combustion, and their interactions. For the time-averaged wall heat flux a sudden rise is observed at about  $x=0.52$ , corresponding well to the location at which the pressure rises due to combustion. The average level in the first part of the combustor agrees well with the laminar heat flux

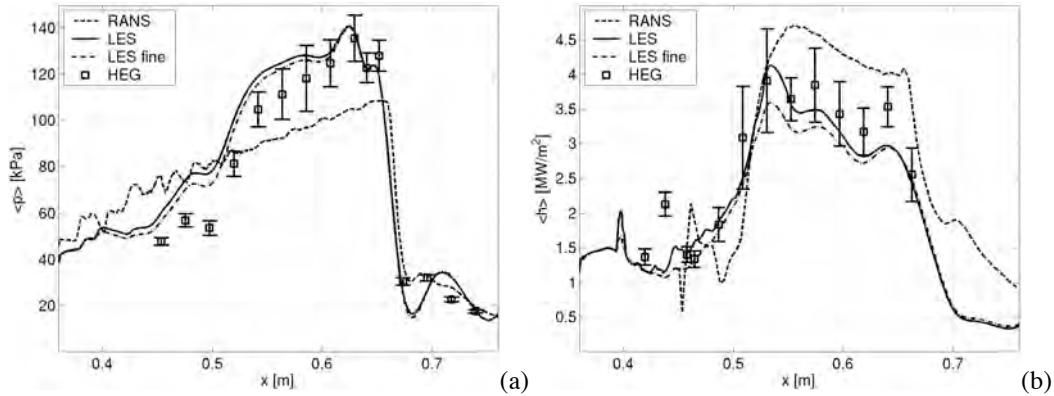


**Figure 6.** Comparison of predicted and measured (a) wall pressure between jet injectors and (b) heat flux along a line 6.0 mm off centerline between jet injectors.

predicted using a Blasius profile and a wall temperature of 300 K, but the transverse  $H_2$  jet introduces some peculiarities after  $x=0.42$ . The RANS predictions typically overpredict the heat flux whereas the LES predictions typically underpredict the heat flux, with between 15% and 10%, respectively. Both the pressure and heat flux predictions are generally within the experimental uncertainty. In addition, the overall combustion efficiency at the outlet is found to be approximately 83%.

In figure 7 we show heat-release, velocity and temperature distributions 1.0 mm above the lower wall in the HyShot II engine. The stoichiometric value of the mixture fraction is superimposed on the heat release to illustrate where heat release may take place according to turbulent diffusion flame theory. Heat release is observed to take place just beneath the bow shocks due to shock ignition, and further downstream where  $H_2$  is sufficiently mixed with air to form a combustible mixture and the thermal

conditions are favorable for self-ignition. Here, self-ignition is supported by recirculating hot combustion products, shock-shock interactions, longer residence time due to the lower flow speed and some H radicals trapped in the low speed flow region. The peak values of the heat release occur in the vicinity of the stoichiometric value of the mixture fraction but is distributed across the entire width of the combustor. Downstream of the heat release region we find that the axial velocity increases slowly throughout the combustor to accelerate more rapidly through the nozzle. The temperature increases slowly along the combustor to drop along the nozzle due to the expansion. These physical flow features are supported by the agreement between predicted and measured wall pressure and heat flux shown in figures 6a and 6b, respectively. From the results we also find that about 80% of the fuel is consumed within the combustor whereas an additional 10% is consumed in the exhaust nozzle.

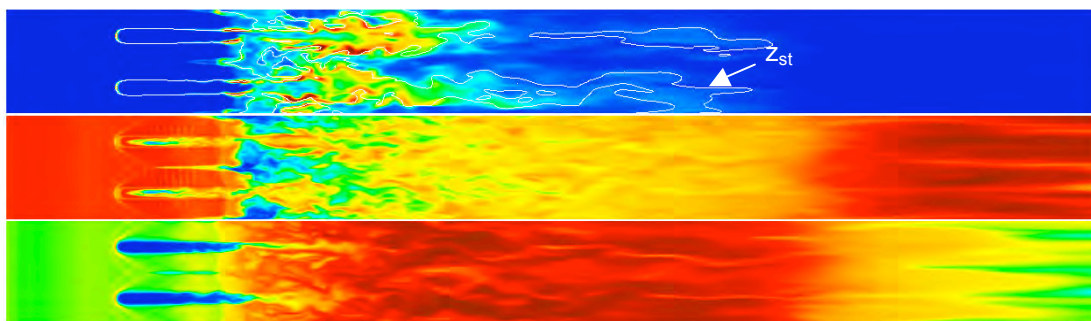


**Figure 7.** Heat-release (top), velocity (middle) and temperature (bottom) distributions 1.0 mm above the lower wall in the HyShot II engine.

## 5. Summary and Concluding Remarks

In this study we use finite rate chemistry LES, using the mixed subgrid scale flow model and the PaSR turbulence chemistry interaction model to study supersonic combustion in a laboratory supersonic combustor and in the HyShot II scramjet engine. The laboratory combustor uses an injection strut to supply  $H_2$  and to stabilize the flame, whereas  $H_2$  is supplied by means of a jet-in-cross-flow configuration for the HyShot II scramjet engine. For both combustor configurations experimental data is available for comparison and thus validation of the computational model. In both cases the LES computations capture the sudden pressure increase caused by the volumetric expansion significant of supersonic combustion well. For the laboratory combustor additional comparisons between measured and predicted OH concentration fields show good agreement, and reveal that the combustion occur primarily in fragmented pockets representative of self-ignition. More precisely, the ‘flame’ is stabilized downstream of the injection strut in a supersonic flow due mainly to self-ignition that gradually transitions into turbulent combustion further downstream. In the case of the HyShot II scramjet combustor additional comparison is made between predicted and measured wall heat fluxes with good overall agreement. In addition to showing good predictive capabilities, without any model parameters to adjust, for two distinctly different scramjet combustors the LES model gives us a unique possibility of visualizing and thus improving our understanding of the interlaced processes of supersonic injection, mixing, self-ignition and combustion necessary for providing sufficient understanding for further development of scramjet engines.

## Acknowledgement

The presented work was supported by the Swedish Armed Forces and the Swedish Defense Material Agency and we also acknowledge the many fruitful discussions with S. Karl, S. Menon and V. Sabelnikov.

## References

- [1] Oevermann M.; 2000, “Numerical Investigation of Hydrogen Combustion in a SCRAMJET using Flamelet Modeling”, *Aerosp. Sci. Tech.* **4**, p 463.
- [2] H. Ebrahimi, F. J. Malo-Molina & D.V. Gaitonde; 2009, “Exploratory RANS and LES Simulations of Transient Supersonic Combustor Flow”, AIAA-0128
- [3] Berglund M., Fedina E., Fureby C., Sabel’nikov V. & Tegnér J.; 2010, “Finite Rate Chemistry Large-Eddy Simulation of Self-Ignition in Supersonic Combustion Ramjet”, *AIAA.J.*, **48**, p 540.
- [4] Sunami T., Magré P., Bresson A., Grisch F., Orain M., & Kodera M.; 2005, “Experimental Study of Strut In-jec-tors in a Supersonic Combustor using OH-PLIF”, AIAA 2005-3304,
- [5] Paull A.; 2002, “The HyShot Flight Program and How it was Developed”, AIAA 2002-5248.
- [6] Smart M.K., Hass N.E. & Paull A.; 2006, “Flight Data Analysis of the HyShot II Flight Experiment”, *AIAA J.*, **44**, p 2366.
- [7] Gardner T., Hannemann, K., Paull, A. & Steelant, J.; 2004, “Ground Testing of the HyShot supersonic combustion flight experiment in HEG”, *Proc. 24th Int. Symp. on Shock Waves*, Beijing.
- [8] Oran E.S. & Boris J.P.; 2001, “Numerical Simulation of Reactive Flow”, Cambridge University Press, Cambridge, UK.
- [9] Poinot T. & Veynante D.; 2001, “Theoretical and Numerical Combustion”, R. T. Edwards, Philadelphia.
- [10] Levine R.D.; 2005, “Molecular Reaction Dynamics”, Cambridge university press.
- [11] Menon S. & Fureby C.; 2010, “Computational Combustion”, In *Encyclopedia of Aerospace Engineering*, Eds. Blockley R. & Shyy W., John Wiley & Sons.
- [12] Bensow R. & Fureby C., 2006, “On the Justification and Extension of Mixed Models in LES”, *J Turbulence* **8**, p N54.
- [13] Baudoin E., Nogenmyr K.J., Bai X.S. & Fureby C.; 2009, “Comparison of LES Models applied to a Bluff Body Stabilized Flame”, AIAA 2009-1178.
- [14] Weller H.G., Tabor G., Jasak H. & Fureby C.; 1997, “A Tensorial Approach to CFD using Object Oriented Techniques“, *Comp. in Physics*, **12**, p 629.
- [15] Davidenko D.M., Gökalp I., Dufour E. & Magre P.; 2006, “Systematic Numerical Study of the Supersonic Combustion in an Experimental Combustion Chamber”, AIAA 2006-7915.
- [16] Sunami T., Murakami A., Kudo K., Kodera M. & Nishioka M.; 2002, “Mixing and Combustion Control Strategies for Efficient Scramjet Operation in Wide Range of Flight Mach Numbers, AIAA 2002-5116,
- [17] Collin G., Dessornes O. & Magre P.; 1997, “Installations d’essais pour les recherches fondamentales en propulsion, PEP/FDP AGARD on Aerospace tech-

nology in the Service of the Alliance, Palaiseau, France.

- [18] Fureby C.; 2007, "On LES and DES of Wall Bounded Flows", *Ercoftac Bulletin* No **72**, Marsh Issue.
- [19] George E., Sebel'nikov V. & Magre P.; 2007, "Large Eddy Simulations and Experimental Study of Self-Ignition of Supersonic Hydrogen and Methane-Hydrogen Jets in a Vitiated Confined Supersonic Air Stream", *Computational combustion*, Delft, The Netherlands.
- [20] Karl S., Hannemann K, Streelant J. & Mack A.; 2006, "CFD Analysis of the HyShot Supersonic Combustion Flight Experiment Configuration", AIAA 2006-8041.
- [21] Gruber M.R., Nejad A.S., Chen T.H. & Dutton J.C.; 1995, "Mixing and Penetration Studies of Sonic Jets in a Mach 2 Freestream", *J. Prop. Power.*, **11**, p 315.
- [22] Ben-Yakar A., Mungal M.G. & Hansen R.K.; 2006, "Time Evolution and Mixing Characteristics of Hydrogen and Ethylene Transverse Jets in Supersonic Crossflows", **18**, p 026101.

### Copyright Statement

The authors confirm that they, and/or their company or organization, hold copyright on all of the original material included in this paper. The authors also confirm that they have obtained permission, from the copyright holder of any third party material included in this paper, to publish it as part of their paper. The authors confirm that they give permission, or have obtained permission from the copyright holder of this paper, for the publication and distribution of this paper as part of the ICAS2010 proceedings or as individual off-prints from the proceedings.